FABAD J. Pharm. Sci., 51, 2, 741-754, 2026
Doi: 10.55262/fabadeczacilik.1920623
RESEARCH ARTICLE

Synthesis and Structural Characterization of Novel Indolin-2-one–Benzimidazole Hybrids with VEGFR-2 Inhibitory Activity

Merve ZENGİN[*°], Emine Merve YILDIRIM[**], Reem K. ARAFA[***]

Synthesis and Structural Characterization of Novel Indolin-2-one–Benzimidazole Hybrids with VEGFR-2 Inhibitory Activity

SUMMARY

In the present study, two indolin-2-one–benzimidazole hybrid compounds were synthesized and structurally characterized by IR, $^{1}H/^{13}C$-NMR, HSQC, NOESY, and HRMS analyses. The cytotoxic activities of the target compounds were evaluated against MCF-7 and MDA-MB-231 breast cancer cell lines, as well as the non-tumorigenic MCF-10A breast epithelial cell line, along with their VEGFR-2 inhibitory activities. Among the synthesized compounds, 2a exhibited potent cytotoxic activity against MCF-7 cells and strong VEGFR-2 inhibition while displaying low toxicity toward MCF-10A cells. Flow cytometric analysis revealed that compound 2a induces apoptosis, whereas ROS analysis indicated only a mild oxidative response. Furthermore, molecular docking studies supported the experimental findings by showing that compound 2a stably binds within the ATP-binding site of VEGFR-2 through key hydrogen bonding and hydrophobic interaction.

Keywords: *Benzimidazole, indolin-2-one, VEGFR-2, molecular docking.*

VEGFR-2 Inhibitör Aktiviteye Sahip Yeni Indolin-2-On–Benzimidazol Hibritlerinin Sentezi ve Yapısal Karakterizasyonu

ÖZ

Bu çalışmada, indolin-2-on–benzimidazol yapısına sahip iki hibrit bileşik sentezlenmiş ve yapıları IR, $^{1}H/^{13}C$-NMR, HSQC, NOESY ve HRMS analizleri ile karakterize edilmiştir. Hedef bileşiklerin sitotoksik aktiviteleri, MCF-7 ve MDA-MB-231 meme kanseri hücre hatlarına ve MCF-10A normal meme epitel hücre hattına karşı değerlendirilmiş; ayrıca VEGFR-2 inhibitör aktiviteleri de incelenmiştir. Sentezlenen bileşikler arasında 2a, MCF-7 hücrelerine karşı güçlü sitotoksik aktivite ve güçlü VEGFR-2 inhibisyonu göstermiş, MCF-10A hücrelerine karşı ise düşük toksisite sergilemiştir. Akış sitometrik analiz, 2a bileşiğinin apoptozu indüklediğini ortaya koyarken; ROS analizi yalnızca hafif bir oksidatif yanıt göstermiştir. Ayrıca moleküler kenetlenme çalışmaları, 2a bileşiğinin temel hidrojen bağları ve hidrofobik etkileşimler aracılığıyla VEGFR-2'nin ATP bağlama bölgesini kararlı bir şekilde işgal ettiğini göstererek deneysel bulguları desteklemiştir.

Anahtar Kelimeler: *Benzimidazol, indolin-2-on, VEGFR-2, moleküler kenetlenme.*

Received: 01.04.2026
Revised: 18.06.2026
Accepted: 09.07.2026

[*] ORCID: 0000-0003-1586-5448, Department of Pharmaceutical Chemistry, Faculty of Pharmacy, Hacettepe University, Ankara, Turkiye
[**] ORCID: 0000-0002-6844-5335, Department of Biochemistry, Faculty of Pharmacy, Hacettepe University, Ankara, Turkiye
[***] ORCID: 0000-0001-7527-1655, Drug Design and Discovery Lab, Zewail City of Science and Technology, Cairo, 12578, Egypt; Biomedical Sciences Program, University of Science and Technology, Zewail City of Science and Technology, Cairo, 12578, Egypt

[°] Corresponding Author; Merve ZENGİN
E-mail: merveozdagli@hacettepe.edu.tr

INTRODUCTION

Cancer has emerged as a highly prevalent and life-threatening disease in recent years. It arises when cells proliferate uncontrollably due to the over-activation, inactivation, or mutation of genes responsible for regulating cell growth and division. Recent advances in targeted therapies have enabled the selective elimination of tumor cells while preserving the viability of normal cells (Min & Lee, 2022; Pérez-Herrero & Fernández-Medarde, 2015). Tyrosine kinases play a crucial role in targeted cancer therapy. Among them, VEGFR-2 is a key mediator of angiogenesis, regulating vascular permeability, endothelial proliferation, migration, and survival. VEGFR-2 inhibition has emerged as a key therapeutic strategy to block tumor angiogenesis, thereby limiting tumor progression and enhancing patient prognosis (Shah et al., 2025). Several VEGFR-2 inhibitors have been approved for clinical use, including axitinib, cabozantinib, lenvatinib, nintedanib, pazopanib, ponatinib, regorafenib, sorafenib, sunitinib, vandetanib, and tivozanib. Although many VEGFR-2 inhibitors have been approved, ongoing studies aim to develop novel agents with improved specificity, reduced adverse effects, and the ability to overcome resistance mechanisms (Marques, Brandão, & Burke, 2024).

Indolin-2-one derivatives have attracted considerable interest owing to their broad pharmacological activities. Numerous studies have reported indolin-2-one-based compounds with anticancer activity, particularly as VEGFR-2 inhibitors (Eldehna et al., 2025; Ezelarab et al., 2024; Qin et al., 2023; Zhang et al., 2014). The indolin-2-one moiety is considered essential because its NH group and carbonyl oxygen serve as a donor–acceptor motif, enabling hydrogen bond interactions with Glu917 and Cys919 in the adenine-binding region of the VEGFR-2 ATP binding site. Sunitinib and nintedanib are clinically approved VEGFR-2 inhibitors containing the indolin-2-one scaffold (Figure 1.) (Yousefian & Ghodsi, 2020).

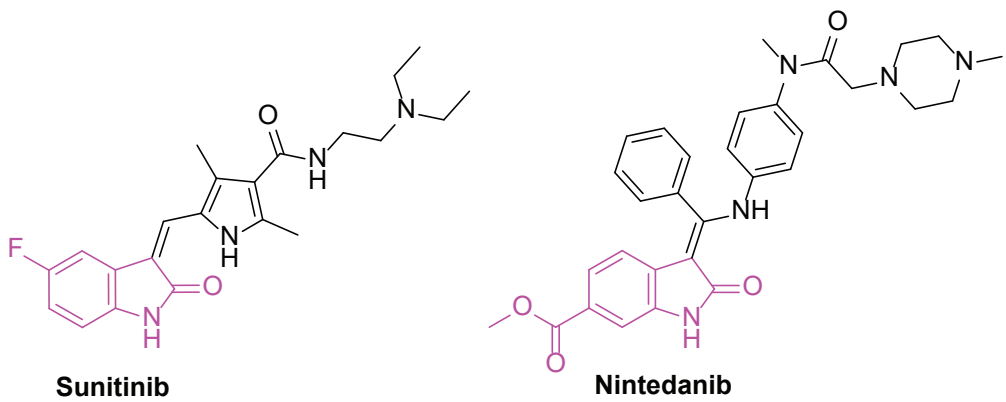

Figure 1. Chemical structures of sunitinib and nintedanib

Benzimidazole is an essential pharmacophore in drug design due to its amphoteric nature and its ability to act as both a hydrogen bond donor and acceptor. This scaffold is associated with diverse biological activities and has gained particular attention in anticancer drug development. Several benzimidazole derivatives exhibit anticancer effects through various mechanisms, and some have been approved for clinical use or are currently under clinical investigation (Mavrova & Yancheva, 2025). Representative examples include dovitinib (Phase III), AT-9283 (Phase II), lifirafenib (Phase I), veliparib and nazartinib (Phase III), which are currently undergoing clinical evaluation, whereas bendamustine, abemaciclib, selumetinib, and binimetinib have been approved for clinical use (Figure 2.).

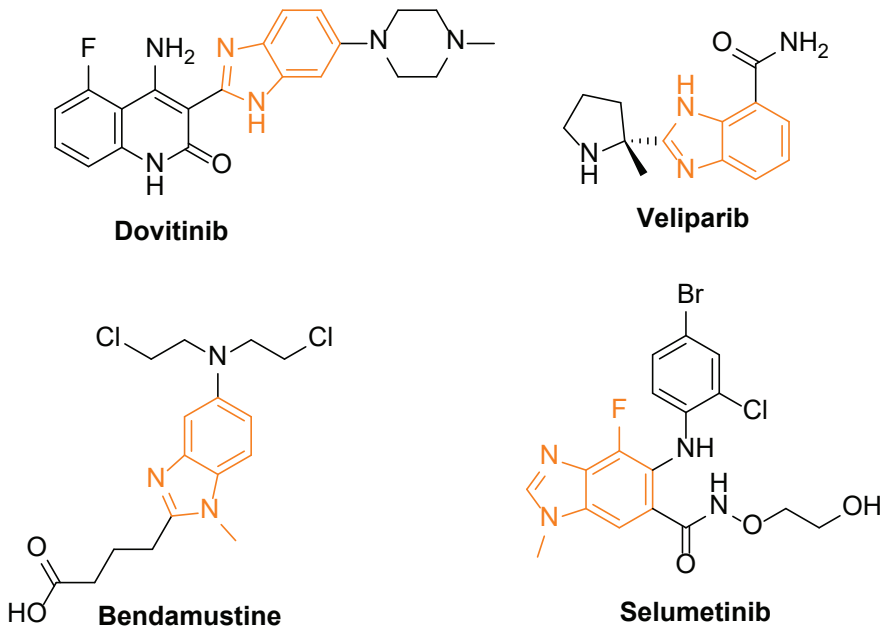

Figure 2. Chemical structures of some anticancer agents containing benzimidazole

Notably, certain benzimidazole derivatives have been reported to exert potent anticancer activity through inhibition of the VEGFR-2 enzyme (Abdel-Mohsen & Nageeb, 2024; Hasegawa et al., 2007; Shokouhi Asl et al., 2025). Research efforts toward the development of novel VEGFR-2 inhibitors remain ongoing. Considering the key pharmacophoric contributions of the indolin-2-one and benzimidazole scaffolds to anticancer activity, two new hybrid compounds were designed. The indolin-2-one scaffold was incorporated to facilitate interactions with the adenine-binding region of the ATP-binding site of VEGFR-2, while the benzimidazole moiety was introduced as a terminal group to enhance the overall molecular properties and promote interactions with the enzyme. Introduction of a chlorine atom at the 6-position of the indolin-2-one ring enabled evaluation of its effect on biological activity (Figure 3.).

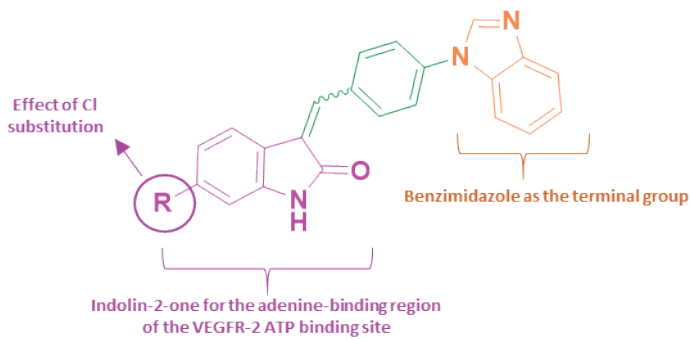

Figure 3. Design of the target compounds

In this study, 3-(4-(1*H*-benzo[*d*]imidazol-1-yl) benzylidene)indolin-2-one **(2a)** and 6-chloro-3-(4-(1*H*-benzo[*d*]imidazol-1-yl)benzylidene)indolin-2-one **(2b)** were synthesized and structurally confirmed using IR, $^{1}H/^{13}C$-NMR, HSQC, NOESY, and HRMS techniques. The compounds were evaluated for their cytotoxic effects against MCF-7 and MDA-MB-231 breast cancer cell lines, as well as the

non-tumorigenic MCF-10A breast epithelial cell line, in addition to their VEGFR-2 inhibitory activities. Furthermore, apoptosis–necrosis and reactive oxygen species assays were performed for compound **2a**, and molecular docking studies were carried out to elucidate its binding mode within the VEGFR-2 active site.

MATERIALS AND METHODS

Chemistry and analysis

All chemicals were purchased from Sigma-Aldrich Chemical Co. (Sigma-Aldrich Corp., St. Louis, MO, USA) and Merck Chemicals (Merck KGaA, Darmstadt, Germany). Melting points of the compounds were determined using a Stuart SMP20 melting point apparatus and are reported as uncorrected values. ATR-FTIR spectra were obtained using a MIRacle ATR accessory (Pike Technologies) coupled with a Spectrum BX FTIR spectrometer (PerkinElmer), and peak positions are reported in cm^{-1}. ^{1}H, ^{13}C NMR, HSQC, and NOESY spectra (in DMSO-d_6) were recorded on a Bruker Avance Neo 500 MHz NMR spectrometer, using TMS as the internal standard. Chemical shifts are reported in parts per million (ppm). The following abbreviations were used to describe peak splitting patterns: s = singlet, d = doublet, t = triplet, m = multiplet, dd = doublet of doublets. Coupling constants (J) are reported in Hz. High-resolution mass spectrometry (HRMS) analyses were performed using an Agilent 1200/6530 LC/MS system equipped with a high-resolution time-of-flight (Q-TOF) detector.

4-(1H-Benzo[d]imidazol-1-yl)benzaldehyde (1)

4-(1*H*-Benzo[*d*]imidazol-1-yl)benzaldehyde was synthesized with 4-fluorobenzaldehyde and 1*H*-benzo[*d*]imidazole using potassium carbonate as a catalyst in DMSO as described in the literature (Zengin, Unsal-Tan, Küçükkılınç, Ayazgok, & Balkan, 2019).

6-Substituted-3-(4-(1H-benzo[d]imidazol-1-yl) benzylidene)indolin-2-one derivatives (2a and 2b)

Indolin-2-one (or 6-chloroindolin-2-one) and 4-(1*H*-benzo[*d*]imidazol-1-yl)benzaldehyde were reacted in the presence of sodium methoxide under heating for 10 hours. At the end of the reaction, the mixture was poured into ice-cold water and acidified with 1 N hydrochloric acid to pH 4–5. The resulting solid was then filtered, dried, and recrystallized from an acetonitrile–water mixture.

(*E*) 3-(4-(1*H*-Benzo[*d*]imidazol-1-yl)benzylidene)indolin-2-one (2a)

Yield 80 %; mp.= 250–251 °C. **IR (cm^{-1}) υ** 3059 (C-H aromatic), 2898, 2827 (C-H aliphatic), 1688 (C=O). **^{1}H NMR (500 MHz, DMSO-d_6, ppm)** δ 10.68 (s, 1H, NH), 8.68 (s, 1H, benzimidazole H_2), 7.97 (d, *J* = 8.5 Hz, 2H, Ar-$H_{2',6'}$), 7.86 (d, *J* = 8.5 Hz, 2H, Ar-$H_{3',5'}$), 7.81 (d, *J*= 7.35 Hz, 1H, benzimidazole H_4), 7.77 (d, *J*= 7.45 Hz, 1H, benzimidazole H_7), 7.70 (s, 1H, =CH–Ar), 7.67 (d, *J*= 7.7 Hz, 1H, oxindole Ar-H_4), 7.39-7.32 (m, 2H, benzimidazole $H_{5,6}$), 7.26 (t, J = 7.45 Hz, 1H, oxindole Ar-H_6), 6.90-6.87 (m, 2H, oxindole Ar-$H_{5,7}$). **^{13}C NMR & HSQC (125 MHz, DMSO-d_6, ppm)** δ 168.59 (C=O), 144.41(benzimidazole-C_{3a}), 143.68 (benzimidazole-C_2), 143.59 (oxindole Ar-C_{7a}), 137.18 (benzimidazole-C_{7a}), 135.05 (C=<u>C</u>H), 134.02 (Ar-$C_{1'}$), 133.23 (Ar-$C_{4'}$), 131.63 (Ar-$C_{2',6'}$), 130.88 (oxindole Ar-C_6), 128.51 (oxindole Ar-C_{3a}), 124.14 (benzimidazole-C_6), 123.99 (Ar-$C_{3',5'}$), 123.18 (benzimidazole-C_5), 123.04 (oxindole Ar-C_4), 121.72 (oxindole Ar-C_5), 121.22 (oxindole Ar-C_3), 120.53 (benzimidazole-C_4), 111.43 (benzimidazole C_7), 110.71 (oxindole Ar-C_7). **HRMS *m/z*** calculated for $C_{22}H_{15}N_3O$ 338.1293 $[M+H]^+$; found 338.1275.

(*E/Z*) 6-Chloro-3-(4-(1*H*-benzo[*d*]imidazol-1-yl)benzylidene)indolin-2-one (2b)

Yield 78 %; mp.= 255–256 °C. **IR (cm^{-1}) υ** 3086 (C-H aromatic), 2832 (C-H aliphatic), 1713 (C=O). **^{1}H NMR (500 MHz, DMSO-d_6, ppm)** δ 10.85 (s, 1H, NH), 8.68 (s, 1H, benzimidazole H_2), 8.64 (d, *J*= 8.6 Hz, 0.67H, Ar-$H_{2',6'}$, *Z* isomer), 7.98-7.96 (m, 1.51H, Ar-$H_{2',6'}$, *E* isomer, =CH–Ar *Z* isomer), 7.86-7.75 (m, 4.76H, Ar-$H_{3',5'}$, benzimidazole H_4, benzimidazole H_7, =CH–Ar *E* isomer), 7.65 (d, *J*= 8.15 Hz, 1H, oxindole Ar-H_4), 7.40-7.33 (m, 2H, benzimidazole $H_{5,6}$), 7.08

(dd, *J*= 8.12, 1.85 Hz, 0.42H, oxindole Ar-H_5 *E/Z* isomer), 6.95-6.92 (m, 1.13H, oxindole Ar-H_5 *E/Z* isomer and oxindole Ar-H_7 *E/Z* isomer), 6.86 (d, *J*= 1.8 Hz, 0.46H, oxindole Ar-H_7 *E/Z* isomer). **^{13}C NMR (125 MHz, DMSO-d_6, ppm)** δ 169.02, 167.52, 144.94, 144.49, 144.44, 143.67, 142,46, 137,84, 137,39, 136.96, 135.96, 134.82, 134.28, 133.73, 133.34, 133.21, 133.12, 131.73, 127.40, 126.57, 124.30, 124.19, 124.15, 124.06, 123.22, 121.91, 121.47, 121.42, 120.55, 120.17, 111.53, 111.46, 110.66, 109.90. **HRMS *m/z*** calculated for $C_{22}H_{14}ClN_3O$ 372.0903 $[M+H]^+$, 374.0874 $[M+H+2]^+$; found 372.0882, 374.0856.

Biological evaluation

***In vitro* VEGFR-2 tyrosine kinase activity assay**

The BPS Bioscience® VEGFR2 Kinase Assay Kit (Catalog # 40325) was utilized to measure VEGFR2 kinase activity using Kinase-Glo® MAX as a detection reagent. Serial dilutions of the test compounds (0.01, 0.1, 1, 10, and 100 µM) were utilized for the assay, and experimental procedures provided by the manufacturer were followed. Tecan | Spark® multimode microplate reader was used for luminescence measurement. Results obtained were employed to construct a dose-response curve from which the IC_{50} values were determined. Results are the average of three independent runs ± SD. Sorafenib and sunitinib were used as positive control reference drugs.

***In vitro* antiproliferative inhibitory assay on MCF-7, MDA-MB-231 and MCF10A cell lines**

The anti-proliferative properties of compounds and the positive control, Doxorubicin (Sigma), were tested against MCF-7, MDA-MB-231, and MCF-10A cell lines utilizing the MTT assay (Mosmann, 1983). All cell lines were obtained from the American Type Culture Collection (ATCC, USA). The cell lines were maintained in Dulbecco's modified Eagle's media (DMEM) supplemented with 10% FBS, 1% L-glutamine, and 1% antibiotics, and MCF-10A cell complete medium (Elabscience CM-0525) at 37 °C in a humidified environment containing 5% CO_2. Cells were seeded in 96-well plates at 5000 cells per well. After 24 hours of incubation, cells were treated with compounds at various doses for another 24 hours at 37 °C. After incubation, 10 µL of MTT reagent (5 mg/mL) was applied to each well. MTT formazan crystals were dissolved in 100 µL DMSO. The relative cell viability was calculated by comparing the absorbance values at 690 nm (for MTT formazan absorbance) and 570 nm (for reference wavelength) of the treated and untreated control groups using a BMG Omega microplate reader. The IC_{50} values were determined with the GraphPad Prism program.

Apoptosis assay

Flow cytometry enables the analysis of suspended cells based on size and granularity, and is widely used to assess parameters such as apoptosis, necrosis, and cell cycle status. Necrotic cells are identified by compromised membrane integrity, allowing uptake of impermeable DNA-binding dyes like 7-AAD. Apoptotic cells are detected via externalization of phosphatidylserine, which binds fluorescently labeled annexin V. For analysis, 1×10^6 compound-treated cells were centrifuged (1200×g, 5 min), washed twice with cold PBS, and resuspended in 500 µl binding buffer. Cells were then stained with 5 µl FITC-conjugated annexin V (10 mg/ml) and 5 µl 7-AAD (50 mg/ml) (Annexin V-FITC/7-AAD Apoptosis Kit, Elabscience, E-CK-A212), followed by a 15 min incubation at room temperature in the dark. Flow cytometric analysis was performed immediately. Cells positive for annexin V alone were considered early apoptotic, while double-positive cells indicated late apoptosis or necrosis.

Reactive oxidative stress (DCFDA) assay

ROS was detected using the ROS Fluorometric Assay Kit (Elabscience, E-BC-K138-F) following the manufacturer's instructions. 2,7-dichlorofluorescin diacetate-DCFDA, a cell-permeable dye, reacts with ROS to generate the highly fluorescent chemical dichlorofluorescein (DCF). Briefly, 1×10^6 compound-treated cells were centrifuged (1200×g, 5 min), washed with PBS, and stained with 25 µM DCFDA.

The cells were then incubated for 30 minutes at 37 °C in an incubator with 5% CO_2. After being washed and resuspended in serum-free medium, the fluorescence intensity was evaluated using flow cytometry.

Molecular docking studies

The crystal structure of VEGFR-2 (PDB ID: 4AGD) was downloaded from the Protein Data Bank (https://www.rcsb.org/structure/4agd). Molecular modeling studies were carried out using AutoDock 4.2 software (Morris et al., 2009). The VEGFR-2 protein was prepared using BIOVIA Discovery Studio 2021 (BIOVIA DS. Dassault Systèmes; San Diego, Release 2021) by removal of water molecules and optimization of the protein structure. The ligands were prepared and minimized with the MM2 force field using Chem 3D Pro 12 software. The files of ligands and protein were converted to a pdbqt file by AutoDock. The binding modes were visualized, and 2D and 3D representations were generated using BIOVIA Discovery Studio 2021.

RESULTS AND DISCUSSION

Chemistry

The synthesis of the target compounds is indicated in Scheme 1. Initially, 4-(1*H*-benzo[*d*]imidazol-1-yl) benzaldehyde (**1**) was prepared by the reaction of 4-fluorobenzaldehyde with 1*H*-benzo[*d*]imidazole in the presence of potassium carbonate. Subsequently, the *Knoevenagel* condensation of indolin-2-one or 6-chloroindolin-2-one with 4-(1*H*-benzo[*d*]imidazol-1-yl)benzaldehyde afforded the target compounds **2a** and **2b** using sodium methoxide as the base, achieving good to excellent yields (78-80%). Structures of target compounds were confirmed using IR, ^{1}H NMR, ^{13}C NMR, HSQC, NOESY, and HRMS analysis.

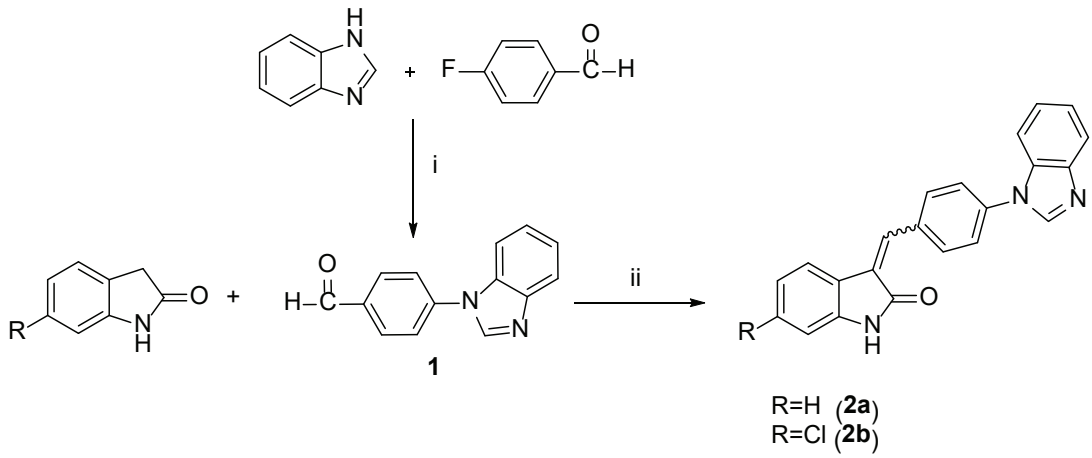

Scheme 1. General procedure for the synthesis of the target compounds; i. K_2CO_3/DMSO/reflux/6h ii. CH_3ONa/CH_3OH/reflux/10h

The presence of an exocyclic double bond in the indolin-2-one derivatives enables the target compounds to exist in *E* and *Z* isomeric forms. These two isomers could be distinguished by ^{1}H-NMR analysis, as they exhibited distinct chemical shifts for Ar-$H_{2',6'}$, the vinyl proton, and oxindole-H_4, consistent with literature (Mansour, Abd El-wahab, Ali, & Aboul-Fadl, 2021; Soudi et al., 2024). In the *Z* isomer, the vinyl protons exhibited a slight downfield shift relative to the *E* isomer, attributed to the deshielding effect of the 2-carbonyl group. Conversely, the Ar-$H_{2',6'}$ resonated at a higher field in the *E* isomer for the same reason. Mansour et al. (2021) reported that the chemical shifts of the major diastereomer (*Z*) showed signals for the vinyl proton at 8.25 ppm, oxindole-H_4 at 8.72 ppm, and Ar-$H_{2',6'}$ at 8.59 ppm, whereas those of the minor diastereomer (*E*) appeared at 7.90, 8.52, and 7.82 ppm, respectively. In the ^{1}H-NMR spectrum of

compound **2a**, the vinyl proton appeared as a singlet at 7.70 ppm, while Ar-$H_{2;6'}$ signals were detected as a doublet at 7.97 ppm, confirming the *E*-configuration of the C=C bond. Additionally, ^{1}H-^{1}H NOE (nuclear overhauser effect spectroscopy [NOESY]) analysis of **2a** revealed NOE interactions between Ar-$H_{3',5'}$ and benzimidazole-H_{2}, benzimidazole-$H_{5,6}$ and $H_{4,7}$, as well as oxindole-$H_{4,6}$ and $H_{5,7}$ protons (Figure 4.).

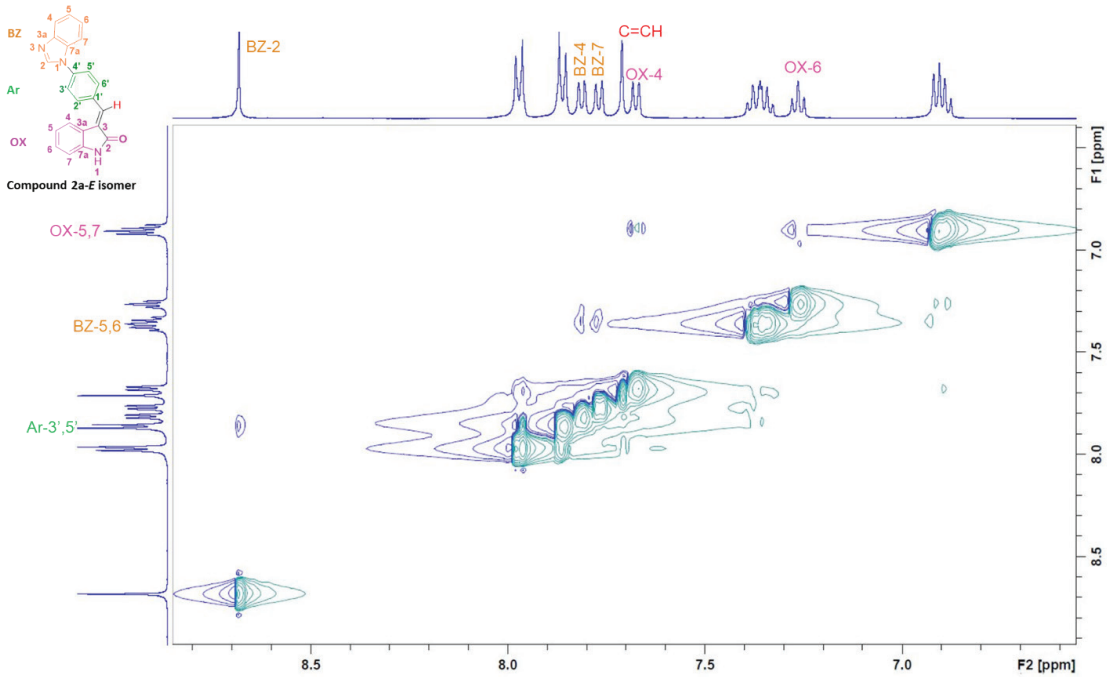

Figure 4. ^{1}H–^{1}H NOESY 2D NMR correlations of compound **2a**

The ^{1}H–^{13}C HSQC was performed for compound **2a**, revealing cross peaks at δH/δC= 8.68/143.68, δH/δC= 7.81/120.53 and δH/δC= 7.77/111.43 ppm corresponding to the H_{2}–C_{2}, H_{4}–C_{4} and H_{7}–C_{7} correlations of the benzimidazole, respectively. Cross peaks at δH/δC=7.67/123.04 and δH/δC=7.26/130.88 ppm were attributed to the H_{4}–C_{4} and H_{6}–C_{6} correlations of the oxindole moiety. Additionally, the two doublet signals at 7.97 and 7.86 ppm, assigned to protons at Ar-$C_{2',6'}$ and Ar-$C_{3',5'}$ displayed cross peaks with the signal at 131.63 and 123.99 ppm, respectively. Finally, the singlet at 7.70 ppm showed a correlation with the signal at 135.05 ppm, corresponding to the vinyl group (Figure 5, Table 1.).

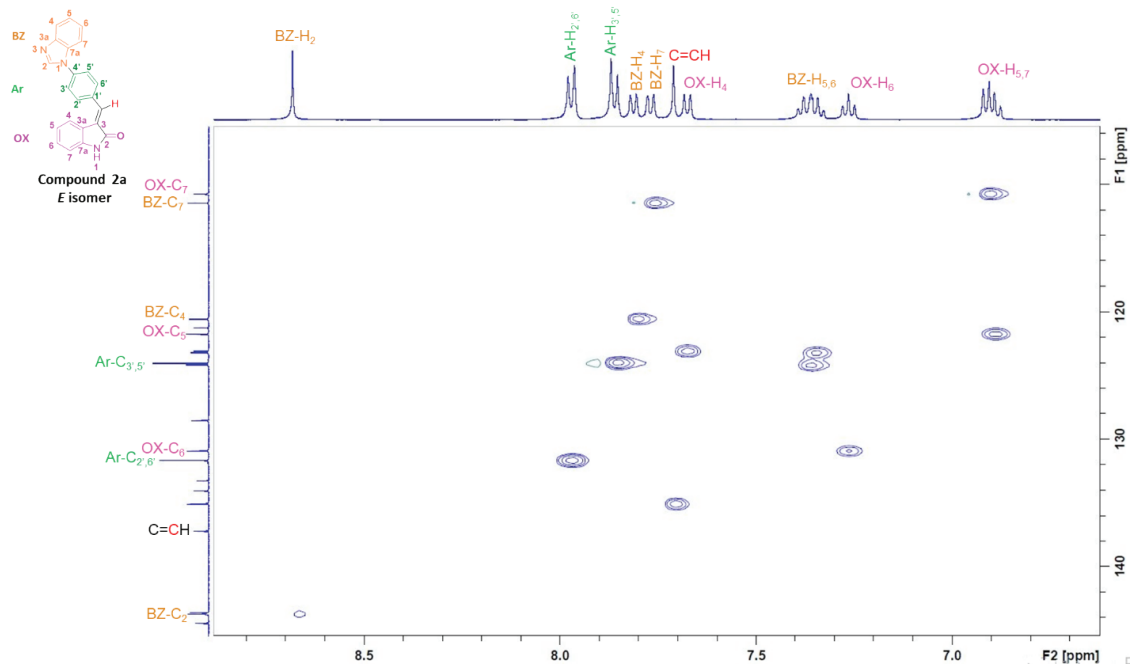

Figure 5. *$^{1}H–^{13}C$ HSQC* NMR correlations of compound **2a**

Table 1. *$^{1}H–^{13}C$ HSQC assignments of compound* **2a**

δH (ppm)	δC (ppm)	Assignment	Moiety
8.68	143.68	$H_2–C_2$	Benzimidazole
7.81	120.53	$H_4–C_4$	Benzimidazole
7.77	111.43	$H_7–C_7$	Benzimidazole
7.67	123.04	$H_4–C_4$	Oxindole
7.26	130.88	$H_6–C_6$	Oxindole
7.97	131.63	Ar-$H_{2',6'}$- $C_{2',6'}$	Phenyl ring
7.86	123.99	Ar-$H_{3',5'}$- $C_{3',5'}$	Phenyl ring
7.70	135.05	C=CH	Vinyl group

Compound **2b** was obtained as a mixture of *E*/*Z*, identified based on the chemical shifts of the Ar-$H_{2',6'}$ protons, which appeared as two distinct doublets at 8.64 and 7.97 ppm, corresponding to the *Z* and *E* configurations, respectively. Furthermore, the vinyl proton, as well as the oxindole-H_5 and H_7 protons, exhibited distinct signals at different chemical shifts due to E/Z isomerism (Figure 6.).

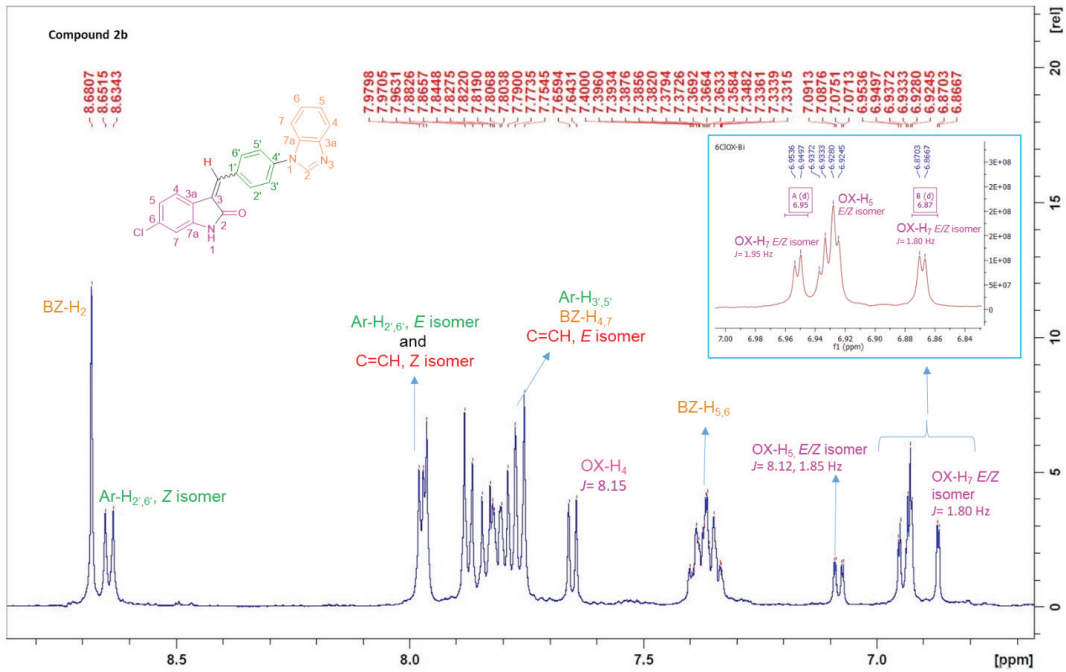

Figure 6. ^{1}H-NMR spectrum of compound **2b**

Biological activity

Cytotoxicity and *in vitro* VEGFR-2 inhibition

The target molecules were evaluated for their cytotoxic effects against the MCF-7 and MDA-MB-231 breast cancer cell lines, as well as the non-tumorigenic MCF-10A breast epithelial cell line, and for their VEGFR-2 inhibitory activities. The results are summarized in Table 2. Compounds **2a** and **2b** exhibited notable cytotoxic activity against the MCF-7 breast cancer cell line, with IC_{50} values of 5.0 and 5.8 μM, respectively, which are more potent than the reference drug doxorubicin (IC_{50}= 6.2 μM). In contrast, both compounds showed lower potency against the MDA-MB-231 cell line, indicating a degree of selectivity toward estrogen receptor-positive breast cancer cells. Notably, compound **2a** showed potent VEGFR-2 inhibitory activity with an IC_{50} value of 0.053 ± 0.002 μM, comparable to sorafenib (IC_{50}= 0.045 ± 0.002 μM), although less potent than sunitinib (IC_{50}= 0.006 μM). The introduction of a chlorine substituent at the 6-position of the indolin-2-one ring resulted in a marked decrease in VEGFR-2 inhibitory activity. Overall, these findings indicate that compound **2a** represents a promising lead structure with cytotoxic and VEGFR-2 inhibitory properties. The compounds did not induce notable cytotoxicity in the non-tumorigenic MCF-10A breast epithelial cells.

Table 2. Cytotoxic effects on breast cell lines and VEGFR-2 inhibitory activities of the compounds

Compound	MCF-7 IC_{50} (μM)*	MDA-MB-231 IC_{50} (μM)*	MCF-10A Cell viability%					VEGFR-2 IC_{50} (μM)#
			100 μM	**20 μM**	**10 μM**	**5 μM**	**1 μM**	
2a	5.0±0.6	20.0±4.6	76.4±9.4	93.3±3.8	94.4±8.7	>100	95.6±7.1	0.053±0.002
2b	5.8±1.0	26.7±8.3	>100	87.7±3.1	80.8±9.2	>100	93.1±9.8	0.764±0.025
Doxorubicine	6.2±1.8	20.3±7.9	>100	89.5±2.0	>100	96.6±12.1	96.4±5.6	
Sunitinib								0.006±0.0001
Sorafenib								0.045±0.002

*Results are the average of three independent runs ± SEM.
#Results are the average of three independent runs ± SD.

Apoptosis analysis

Flow cytometric analysis was performed to investigate the mechanism of action of compound **2a**, selected for its potent activity. Apoptosis was evaluated using Annexin V-FITC/7-AAD double staining to determine viable, early apoptotic, late apoptotic, and dead cell populations in MCF-7 cells after 24 h of treatment. Compound **2a** significantly induced apoptosis, increasing early apoptotic cells (Q1-LR) from 9.5% to 22.2% and late apoptotic cells (Q1-UL) from 1.1% to 24.1% (Figure 7.).

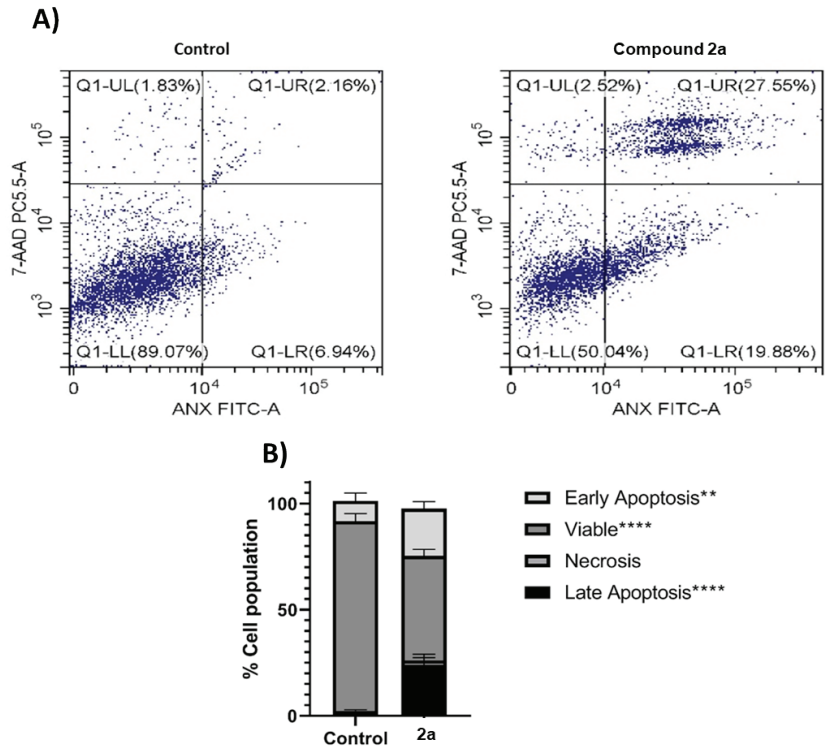

Figure 7. A) Apoptosis and necrosis evaluation of control and **2a** in MCF-7 cancer cells. Q1-LL: viable cells, Q1-LR: early apoptosis, Q1-UR: late apoptosis, Q1-UL: necrosis. B) Graphical representation of the apoptotic effects of **2a** on MCF-7 cells compared to control. Two-way ANOVA followed by Sidak's multiple comparison test was performed to determine statistical significance. P value indicates a significant difference compared with control (**p<0.01, ****p < 0.0001)

Reactive oxidative species

The 2′,7′-dichlorodihydrofluorescein diacetate (DCFDA) assay was performed to measure reactive oxygen species (ROS) levels in MCF-7 cells after 24-hour treatment with compound **2a** at its IC_{50} concentration. As shown in Table 3, the corrected mean fluorescence intensity (MFI) for ROS in the compound **2a**-treated group was 106.9 ± 1.2%, representing a slight increase compared to the control group (100±0.3%), though statistical significance was not specified. In contrast, the positive control tert-butyl hydroperoxide (THBP) exhibited a significantly higher median fluorescence intensity (MFI) of 114.7±3.4% (p<0.01). Notably, the percentage of ROS-positive cells decreased significantly in the compound **2a**-treated group (27.7±1.0%, p<0.05) compared to the control group (37.8±1.3%), while the positive control showed an increase to 42.5±4.2% (Figure 8.). However, the reduced percentage of ROS-positive cells in the treated group suggests that although the overall oxidative burden increases, it is more uniformly distributed among the surviving

cells, or that a subpopulation with high ROS may have undergone apoptosis. This finding suggests that the pro-apoptotic action of compound **2a** is not strongly associated with ROS accumulation and may be mediated by ROS-independent mechanisms, such as inhibition of survival signaling pathways (e.g., PI3K/Akt, VEGFR-2), although a mild oxidative contribution cannot be fully excluded.

Table 3. Impact of compound **2a** and positive control (THBP) on intracellular ROS production

	Corrected % MFI			**% Cell population**	
	Mean± SEM	Statistical significance		**Mean± SEM**	Statistical significance
Control	100±0.3			37.8±1.3	
Compound 2a	106.9±1.2			27.7±1.0	*
Positive Control (THBP)	114.7±3.4	**		42.5±4.2	

[a] The results are supplied as mean ± SEM of 3 experiments. *p < 0.05, **p<0.01 indicate the significance of the obtained values statistically.

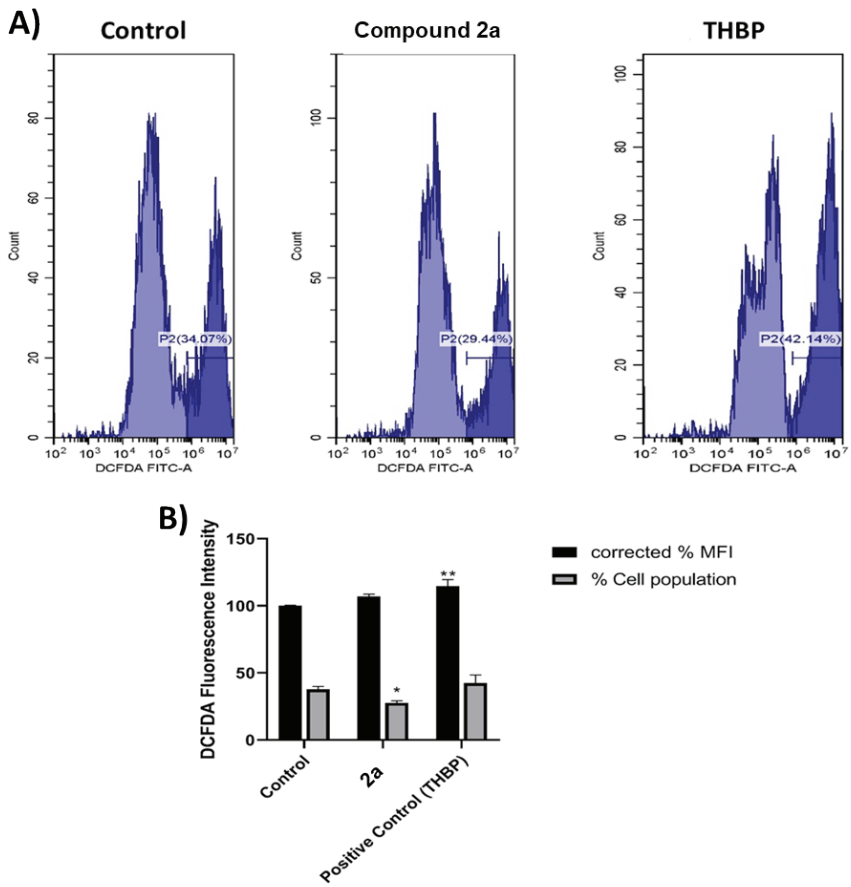

Figure 8. A) Flow cytometry histograms showing changes in ROS levels. (B) Graphical representation of ROS production in response to the effects of control, compound 2a, and THBP. One-way ANOVA followed by Dunnett's test was performed to determine statistical significance. P-value indicates a significant difference compared with control (*p<0.05, **p<0.01)

Molecular docking studies

Molecular docking studies were performed using AutoDock 4.2 to examine the potential binding mode of compound **2a** within the ATP-binding domain of the VEGFR-2 active site (PDB ID: 4AGD). The docking protocol was validated by re-docking the co-crystallized sunitinib, resulting in an RMSD value of 0.98 Å, which confirmed the validity of the docking procedure. Docking results suggested that compound **2a** binds within the ATP-binding domain of VEGFR-2 through strong key interactions. The indolin-2-one scaffold formed two hydrogen bonds with Glu917 and Cys919 via its NH and carbonyl (C=O) groups and also engaged in multiple hydrophobic interactions with Val848, Ala866, Leu1035, and Cys1045. The central benzylidene moiety established hydrophobic interactions with Leu840, while the terminal benzimidazole formed van der Waals interactions with Gly841, Gly922, Asn923, Arg1032, and Arg1051 (Table 4, Figure 9.). It may be concluded that these interactions are likely important for maintaining the stability of the ligand–protein complex.

Table 4. Molecular docking interactions of compound **2a** with the VEGFR-2 active site

Compound	VEGFR-2 binding energy (ΔG kcal/mol)	Main residue	Type of interaction	Bond distance (Å)
2a	-10.53	Glu917	H-bond	2.11
		Cys919	H-bond	2.69
		Val848	π-alkyl	5.06
		Ala866	π-alkyl	4.87
		Leu1035	π-sigma	3.57
		Cys1045	π-alkyl	4.76
		Leu840	π-alkyl	5.22
		Phe1047	π - π	4.59

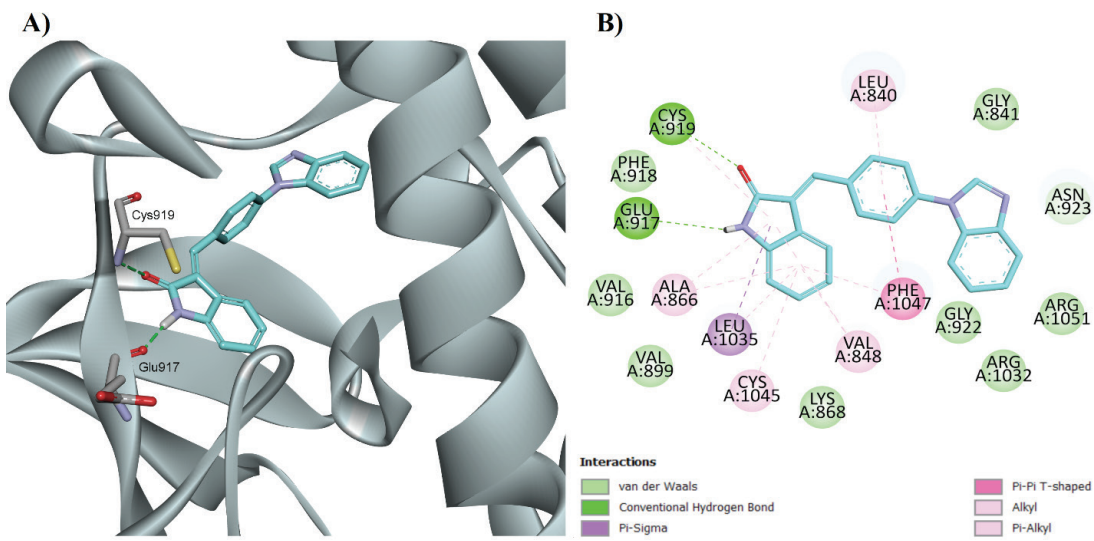

Figure 9. 3D and 2D representations of the binding mode of **2a** in the VEGFR-2 active site

CONCLUSION

In this study, 3-(4-(1*H*-benzo[*d*]imidazol-1-yl) benzylidene)indolin-2-one (**2a**) and 6-chloro-3-(4-(1*H*-benzo[*d*]imidazol-1-yl)benzylidene)indolin-2-one (**2b**) were successfully synthesized and structurally characterized by IR, $^{1}H/^{13}C$-NMR, HSQC, NOESY, and HRMS analyses. Compound **2a** emerged as a promising lead molecule, exhibiting potent cytotoxic activity against MCF-7 breast cancer cells and strong VEGFR-2 inhibitory efficacy, while maintaining low toxicity toward non-tumorigenic MCF-10A cells. Flow cytometric analysis confirmed that the cytotoxic effect of compound **2a** is primarily mediated through apoptosis induction. ROS analysis indicated only a mild oxidative response, suggesting that oxidative stress is not the dominant mechanism of action. Molecular docking studies further supported the experimental findings by suggesting a favorable binding mode of compound **2a** within the ATP-binding site of VEGFR-2 through key hydrogen-bonding and hydrophobic interactions. Overall, **2a** represents a promising lead candidate for further optimization as a VEGFR-2 inhibitor for the development of potential anti-breast cancer agents.

ACKNOWLEDGEMENT

This work was supported by the Scientific Research Fund of Hacettepe University, Turkey through Project THD-2022-19967.

AUTHOR CONTRIBUTION STATEMENT

M.Z.: Investigation, methodology, software, writing original draft, writing–review and editing; E.M.Y.: methodology, writing–review and editing; R.K.A.: methodology, writing–review and editing.

CONFLICT OF INTEREST

The authors declare that there is no conflict of interest.

REFERENCES

Abdel-Mohsen, H. T., & Nageeb, A. M. (2024). Benzimidazole–dioxoisoindoline conjugates as dual VEGFR-2 and FGFR-1 inhibitors: design, synthesis, biological investigation, molecular docking studies and ADME predictions. *RSC Advances, 14*(39), 28889-28903. doi:http://dx.doi.org/10.1039/D4RA05462H

BIOVIA DS. Dassault Systèmes; San Diego, Release 2021.

Eldehna, W. M., Tawfik, H. O., Nafie, M. S., Al Kamaly, O., El-Hamaky, A. A., El Hassab, M. A., . . . Balaha, M. (2025). Novel benzofuran-conjugated indolin-2-ones as anticancer agents: design, synthesis, biological assessments, and molecular modeling insights. *Bioorganic Chemistry, 160*, 108494. doi:https://doi.org/10.1016/j.bioorg.2025.108494

Ezelarab, H. A. A., Abd El-Hafeez, A. A., Ali, T. F. S., Sayed, A. M., Hassan, H. A., Beshr, E. A. M., & Abbas, S. H. (2024). New 2-oxoindole derivatives as multiple PDGFRα/ß and VEGFR-2 tyrosine kinase inhibitors. *Bioorganic Chemistry, 145*, 107234. doi:https://doi.org/10.1016/j.bioorg.2024.107234

Hasegawa, M., Nishigaki, N., Washio, Y., Kano, K., Harris, P. A., Sato, H., . . . Cheung, M. (2007). Discovery of Novel Benzimidazoles as Potent Inhibitors of TIE-2 and VEGFR-2 Tyrosine Kinase Receptors. *Journal of Medicinal Chemistry, 50*(18), 4453-4470. doi:https://doi.org/10.1021/jm0611051

Mansour, H. S., Abd El-wahab, H. A. A., Ali, A. M., & Aboul-Fadl, T. (2021). Inversion kinetics of some E/Z 3-(benzylidene)-2-oxo-indoline derivatives and their in silico CDK2 docking studies. *RSC Advances, 11*(14), 7839-7850. doi:http://dx.doi.org/10.1039/D0RA10672K

Marques, C. S., Brandão, P., & Burke, A. J. (2024). Targeting Vascular Endothelial Growth Factor Receptor 2 (VEGFR-2): Latest Insights on Synthetic Strategies. *Molecules, 29*(22), 5341. Retrieved from https://www.mdpi.com/1420-3049/29/22/5341

Mavrova, A., & Yancheva, D. (2025). Benzimidazole-based hybrids as inhibitors of EGFR/VEGFR-2 and their combinations with other enzymes: design, synthesis, and activity. *Bioorganic Chemistry, 164*, 108920. doi:https://doi.org/10.1016/j.bioorg.2025.108920

Min, H.-Y., & Lee, H.-Y. (2022). Molecular targeted therapy for anticancer treatment. *Experimental & Molecular Medicine, 54*(10), 1670-1694. doi:https://doi.org/10.1038/s12276-022-00864-3

Morris, G. M., Huey, R., Lindstrom, W., Sanner, M. F., Belew, R. K., Goodsell, D. S., & Olson, A. J. (2009). AutoDock4 and AutoDockTools4: Automated docking with selective receptor flexibility. *Journal of Computational Chemistry, 30*(16), 2785-2791. doi:https://doi.org/10.1002/jcc.21256

Mosmann, T. (1983). Rapid colorimetric assay for cellular growth and survival: application to proliferation and cytotoxicity assays. *J Immunol Methods, 65*(1-2), 55-63. doi:https://doi.org/10.1016/0022-1759(83)90303-4

Pérez-Herrero, E., & Fernández-Medarde, A. (2015). Advanced targeted therapies in cancer: Drug nanocarriers, the future of chemotherapy. *European Journal of Pharmaceutics and Biopharmaceutics, 93*, 52-79. doi:https://doi.org/10.1016/j.ejpb.2015.03.018

Qin, Q., Fu, Q., Wang, X., Lv, R., Lu, S., Guo, Z., . . . Cheng, M. (2023). Design, synthesis and biological evaluation of novel indolin-2-one derivatives as potent second-generation TRKs inhibitors. *European Journal of Medicinal Chemistry, 253*, 115291. doi:https://doi.org/10.1016/j.ejmech.2023.115291

Shah, F. H., Nam, Y. S., Bang, J. Y., Hwang, I. S., Kim, D. H., Ki, M., & Lee, H.-W. (2025). Targeting vascular endothelial growth receptor-2 (VEGFR-2): structural biology, functional insights, and therapeutic resistance. *Archives of Pharmacal Research, 48*(5), 404-425. doi:https://doi.org/10.1007/s12272-025-01545-1

Shokouhi Asl, A. S., Ranjbar, S., Sayahi, M. H., Dehghani, Z., Taherkhani, A. M., Negahdaripour, M., . . . Ghasemi, Y. (2025). Synthesis, biological evaluation, and docking analysis of novel benzimidazole–triazole hybrids as potential anticancer agents. *RSC Advances, 15*(44), 37447-37460. doi:http://dx.doi.org/10.1039/D5RA02760H

Soudi, A., Bender, O., Celik, I., El-Hafeez, A. A. A., Dogan, R., Atalay, A., . . . Ali, T. F. S. (2024). Discovery and Anticancer Screening of Novel Oxindole-Based Derivative Bearing Pyridyl Group as Potent and Selective Dual FLT3/CDK2 Kinase Inhibitor. *Pharmaceuticals, 17*(5), 659. doi:https://www.mdpi.com/1424-8247/17/5/659

Yousefian, M., & Ghodsi, R. (2020). Structure–activity relationship studies of indolin-2-one derivatives as vascular endothelial growth factor receptor inhibitors and anticancer agents. *Archiv der Pharmazie, 353*(12), 2000022. doi:https://doi.org/10.1002/ardp.202000022

Zengin, M., Unsal-Tan, O., Küçükkılınç, T. T., Ayazgok, B., & Balkan, A. (2019). Design and Synthesis of 2-Substitutedphenyl Benzo[D]Thiazole Derivatives and Their β-Amyloid Aggregation and Cholinesterase Inhibitory Activities. *Pharmaceutical Chemistry Journal, 53*(4), 322-328. doi:https://doi.org/10.1007/s11094-019-02000-4

Zhang, L., Zheng, Q., Yang, Y., Zhou, H., Gong, X., Zhao, S., & Fan, C. (2014). Synthesis and in vivo SAR study of indolin-2-one-based multi-targeted inhibitors as potential anticancer agents. *European Journal of Medicinal Chemistry, 82*, 139-151. doi:https://doi.org/10.1016/j.ejmech.2014.05.051